Submicron separation of microspheres via travelling surface acoustic waves

Ghulam Destgeer, Byung Hang Ha, Jin Ho Jung and Hyung Jin Sung*

Department of Mechanical Engineering, KAIST, 291 Daehak-ro, Yuseong-gu, Daejeon 305-701, Korea. Email: hjsung@kaist.ac.kr.

Tab. S1 The values of κ factor computed against frequency f and particle diameter d_p used in the present study

f (MHz) / d_p (µm)	κ						
	0.71	3.0	3.2	3.4	4.2	4.5	5.0
129	0.19	0.81	0.86	0.92	1.13	1.22	1.35
155	0.23	0.97	1.04	1.1	1.36	1.47	1.62
192	0.29	1.21	1.29	1.37	1.69	1.82	2.01
200	0.3	1.26	1.34	1.42	1.76	1.89	2.09

Theoretical Models:

The *rigid* and *elastic theories* are summarized below and were used to estimate the acoustic radiation force factor (ARFF) acting on polystyrene (PS) particles suspended in water.

Rigid theory: The ARF (F_R) acting on a rigid sphere is a function of the fluid and particle density ratio and size of the particle relative to the wavelength of wave and is defined as:

$$F_R = \pi a^2 \cdot \overline{E} \cdot F_F \tag{S1}$$

The sound energy density ($\overline{E}$) in the fluid is defined as:

$$\overline{E} = \frac{1}{2}\rho_f k |A|^2 \tag{S2}$$

where ρ_f is the density of fluid and A is the complex amplitude of velocity potential function related with the amplitude of sound wave. ARFF (F_F) is a dimensionless parameter defined as the force per unit area (πa^2) per unit sound energy density ($\overline{E}$). The ARFF for a plane travelling wave is defined as:

$$F_F = \frac{4}{\kappa^4}\left[\frac{1}{L_0 L_1} + \frac{2\{\kappa^2 - 3(1-\chi)\}^2}{\kappa^8 L_1 L_2} + \sum_{n=2}^{\infty}\frac{(n+1)}{\kappa^{4(n+1)}}\times\frac{(\kappa^2 - n(n+2))^2}{L_n L_{n+1}}\right] \tag{S3}$$

and for a standing wave:

$$F_F = \frac{2}{\kappa^3}\left[\frac{K_0}{L_0 L_1} - \frac{2K_1\{\kappa^2 - 3(1-\chi)\}}{\kappa^4 L_1 L_2} + \sum_{n=2}^{\infty}\frac{(-1)^n (n+1)}{\kappa^{2(n+1)}}\times\frac{K_n(\kappa^2 - n(n+2))}{L_n L_{n+1}}\right]\cdot\sin(2kh) \tag{S4}$$

where

$$K_0 = \sqrt{L_0 L_1 - \frac{1}{\kappa^2}} \tag{S5a}$$

$$K_1 = \sqrt{L_1 L_2 - \frac{\left(\kappa^2 - 3(1-\chi)\right)^2}{\kappa^{10}}} \tag{S5b}$$

$$K_n = \sqrt{L_n L_{n+1} - \frac{\left(\kappa^2 - n(n+2)\right)^2}{\kappa^{4n+6}}} \tag{S5c}$$

$$L_1 = \frac{\pi}{2\kappa^3}\left[(1-\chi)^2 \cdot \left(J_{1.5}^2 + J_{-1.5}^2\right) + 2\kappa \cdot (1-\chi) \cdot \left(J_{-1.5} J_{-2.5} - J_{1.5} J_{2.5}\right) + \kappa^2 \cdot \left(J_{2.5}^2 + J_{-2.5}^2\right)\right] \tag{S5d}$$

$$L_n = \frac{\pi}{2\kappa^{2n+1}}\left[n^2 \cdot \left(J_{n+0.5}^2 + J_{-n-0.5}^2\right) + 2n\kappa \cdot \left(J_{-n-0.5} J_{-n-1.5} - J_{n+0.5} J_{n+1.5}\right) + \kappa^2 \cdot \left(J_{n+1.5}^2 + J_{-n-1.5}^2\right)\right] \tag{S5e}$$

for $n \neq 1$

and,

$$\chi = \frac{\rho_f}{\rho_s} \tag{S5f}$$

To simplify the comparison, the value of $\sin(2kh)$ is assumed to be one, where h is the distance between the particle and an acoustic pressure node. ρ_s is the density of the sphere. J_n is the spherical Bessel functions of the first kind of order n, with values that may be calculated for various κ using the above equations.

Tab. S2 Properties of materials

Properties	Units	Water	Polystyrene	Fused Silica
Density	kg/m^3	998	1050	2214
Speed of sound (longitudinal)	m/s	1495	2350	5950
Speed of sound (shear)	m/s	-	1120	3750
Poison ratio	-	-	0.35	0.17

The ARF factor using King's rigid theory for travelling and standing waves and their ratio is plotted against κ in Fig. S1. The microsphere material is assumed to be PS and liquid media is water. The properties of the water and particles used is listed in Tab. S2. The critical value of κ (when ARFF ratio is equal to 1) for the PS particles is approximately 1.05 (for simplicity we say it is equal to 1). The reason behind plotting Fig. S1 is to find out the regions of dominance for travelling and standing waves. Although the behaviour of the PS particles could not be predicted accurately using the *rigid theory* (PS particles are far from rigid), a reasonable qualitative model of the ARFF could be calculated. The ratio of the force factors (F_F) estimated for standing and travelling waves returned a value much higher than 1 for $\kappa \ll 1$, indicating the region in which the ARF produced by standing waves was dominant. For $\kappa \gtrsim 1$, the travelling waves' effects became more prominent.
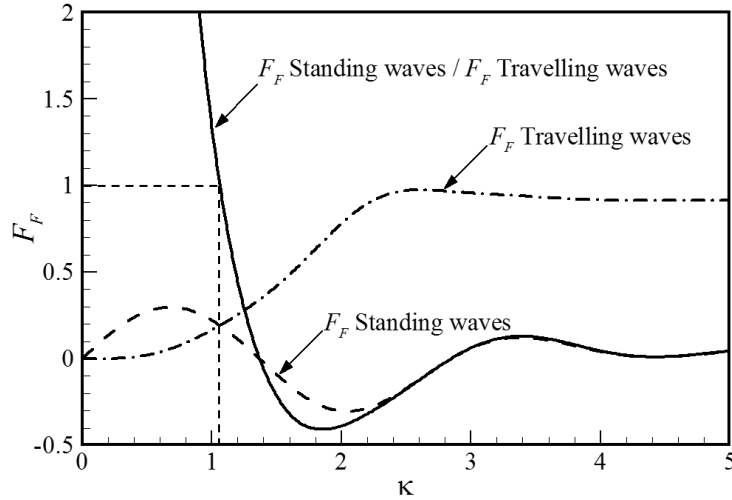
Fig. S1 The ARF factors for travelling and standing waves are plotted as a function of κ. The ratio of the factors indicated that the standing waves were dominant for $\kappa \lesssim 1$, and the TSAW was dominant for $\kappa \gtrsim 1$.

Elastic theory: The force factor (F_F) for a plane travelling wave interacting with a sphere includes the effects of the compressibility and the elasticity of a particle and is defined as:

$$F_F = \frac{4}{\kappa^2} \sum_{n=0}^{\infty} \begin{bmatrix} (n+1)\cdot(P'_{n+1}\cdot Q'_n - P'_n\cdot Q'_{n+1})\cdot \kappa_f{}^2 - n\cdot(n+1)\cdot(n+2)\cdot(P_{n+1}\cdot Q_n - P_n\cdot Q_{n+1}) \\ +(n\cdot(n+1)\cdot(P_{n+1}\cdot Q'_{n+1} - P'_{n+1}\cdot Q_n) - (n+1)\cdot(n+2)\cdot(P'_n\cdot Q_{n+1} - P_{n+1}\cdot Q'_n))\cdot \kappa \\ +(n+1)\cdot(P_{n+1}\cdot Q_n - P_n\cdot Q_{n+1})\cdot \kappa^2 \end{bmatrix},$$

(S6)

where,

$$P_n = (1+M_n)\cdot J_n + N_n\cdot Y_n \tag{S7a}$$

$$P'_n = (1+M_n)\cdot J'_n + N_n\cdot Y'_n \tag{S7b}$$

$$Q_n = N_n\cdot J_n - M_n\cdot Y_n \tag{S7c}$$

$$Q'_n = N_n\cdot J'_n - M_n\cdot Y'_n \tag{S7d}$$

where,

$$M_n = -\frac{[R_n\cdot J_n - \kappa\cdot J'_n]^2}{[R_n\cdot J_n - \kappa\cdot J'_n]^2 + [R_n\cdot Y_n - \kappa\cdot Y'_n]^2} \tag{S8a}$$

$$N_n = -\frac{[R_n\cdot J_n - \kappa\cdot J'_n]\cdot[R_n\cdot Y_n - \kappa\cdot Y'_n]}{[R_n\cdot J_n - \kappa\cdot J'_n]^2 + [R_n\cdot Y_n - \kappa\cdot Y'_n]^2} \tag{S8b}$$

where,

$$R_n = \frac{\chi\cdot\kappa_2^2}{2}\cdot\frac{\dfrac{\kappa_1\cdot J'_n(\kappa_1)}{\kappa_1\cdot J'_n(\kappa_1) - J_n(\kappa_1)} - \dfrac{2\cdot n\cdot(n+1)\cdot J_n(\kappa_2)}{(n+2)\cdot(n-1)\cdot J_n(\kappa_2) + \kappa_2^2\cdot J''_n(\kappa_2)}}{\dfrac{\kappa_1^2\cdot[(\sigma/(1-2\sigma))\cdot J_n(\kappa_1) - J''_n(\kappa_1)]}{\kappa_1\cdot J'_n(\kappa_1) - J_n(\kappa_1)} - \dfrac{2\cdot n\cdot(n+1)\cdot[J_n(\kappa_2) - \kappa_2\cdot J'_n(\kappa_2)]}{(n+2)\cdot(n-1)\cdot J_n(\kappa_2) + \kappa_2^2\cdot J''_n(\kappa_2)}} \tag{S9}$$

$$\kappa_1 = k_1\cdot a = \frac{2\pi\cdot f}{c_1}\cdot a \tag{S10a}$$

$$\kappa_2 = k_2 \cdot a = \frac{2\pi \cdot f}{c_2} \cdot a \qquad\qquad\qquad (S10b)$$

The wavenumbers k_1 and k_2 and sound velocities in elastic sphere c_1 and c_2 correspond to longitudinal (or compressional) waves and shear waves propagating inside the particle, respectively. σ is the Poisson ratio and Y_n is the spherical Bessel function of the second kind and order n. The first and second derivatives of the spherical Bessel functions are calculated as,

$$J_n'(x) = \frac{n}{x} \cdot (J_n(x) - J_{n+1}(x)) \qquad\qquad\qquad (S12a)$$

$$J_n''(x) = \frac{n}{x^2} \cdot (xJ_n'(x) - J_n(x)) - J_{n+1}'(x) \qquad\qquad\qquad (S12b)$$

The ARFF is estimated by using both the rigid and elastic theories for fused silica (FS) and PS particles suspended in water, as plotted in Fig. S2. First, to validate the computational models, the ARFF was computed for FS particles and compared with a previous study by Hasegawa et al., which shows a good agreement. The ARFF is then calculated for PS particles using the rigid theory which shows a similar behaviour as FS. However, the lower density contrast of PS with the carrier fluid results in the lower ARF values. The force factor (F_F) curve for PS particles by the elastic theory shows a very steep slope after the κ values exceeding 1. As the PS particle were less dense and more compressible than FS, the results obtained from the elastic theory deviates from those obtained from the rigid theory. The *elastic* theory predictions appeared to better approximate the experimental behaviour.
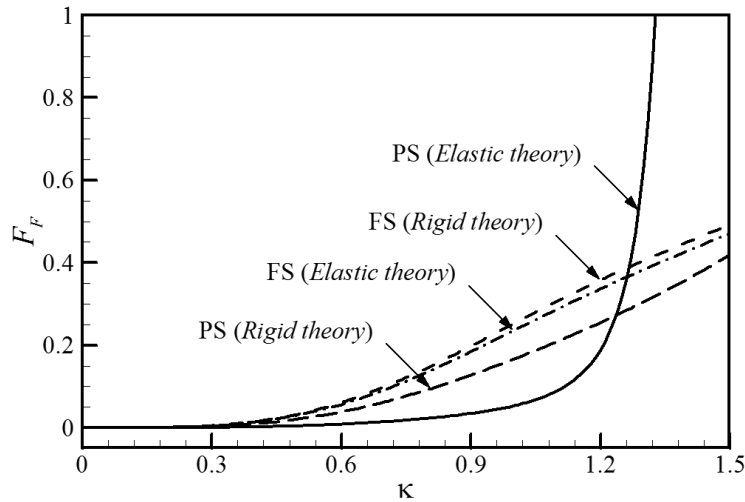
Fig. S2 The ARF factors obtained from FS and PS particles are plotted as a function of κ. The curves computed using the elastic or rigid theories for the FS particles agreed well with the present range of κ; however, for PS particles, the results differed significantly.

The ARF factor for PS particles suspended in water is then estimated for different frequencies over a range of particle diameters and κ shown in Fig. S3. The steep slope of the curve indicates that the acoustic radiation force acting on a PS particle increases abruptly with little increase in κ which in turn suggests minute increase in particle diameter or acoustic wave's frequency. Considering that PS is a purely elastic material, such behaviour of PS elastic particles indicates that the separation of particles with a very little size difference is possible if sound waves of a suitable frequency are used. Sound waves with frequency 129, 155 and 192 MHz can be chosen for effective submicron separation of particles with diameter that ranges within 4-5 μm, 3.2-4.2 μm and 2.4-3.4 μm, respectively. These ranges roughly correspond to $1.0 < \kappa < 1.4$. It is

even easier to separate particles with a larger size difference. The experimental separation of various size particles with many size differences is discussed in the results section.
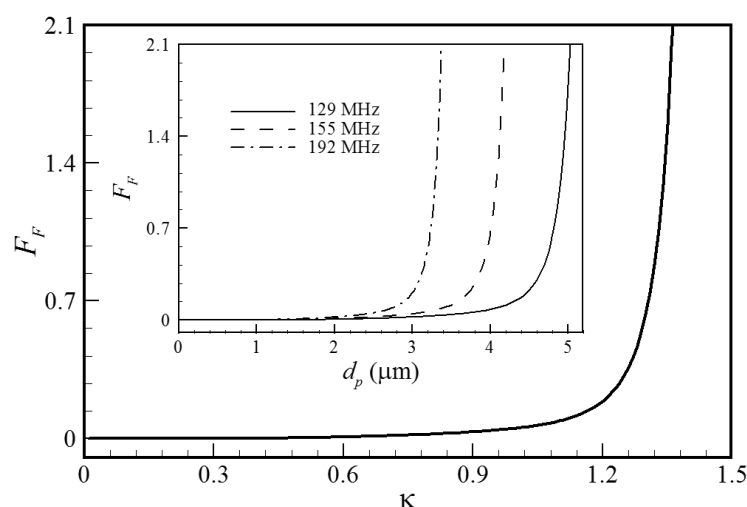
Fig. S3 The ARF factor for PS particles is plotted against κ. The inset shows F_F dependence on particle diameter for three difference frequencies.

Movie Captions:

Movie I: The separation of 0.71 µm particles from 3.0 µm particles is demonstrated. The net flow rate was 130 µL/h, whereas the microchannel dimensions (w x h) at the separation zone were 200 µm x 40 µm. The particles were flowing together in a laminar flow as the TSAW were OFF, however, a significant separation distance was induced as the TSAW were turned ON.

Movie II: The separation zone of the microchannel is shown. The separation of 3.0 µm particles from 3.2 µm (red fluorescent) particles was achieved by 200 MHz TSAW. Dark field imaging is used along with fluorescence microscopy to distinguish red fluorescent particles from non-fluorescent particles. The fluorescent particles always appeared brighter. The non-fluorescent particles disappear from the frame as the microscope lamp was turned off. As the difference in average diameters of particles was very small, this simple technique was used to distinguish the fluorescent particles from non-fluorescent particles in a continuous flow.

Movie III: The outlet zone of the microchannel is shown. The sorting of 3.0 µm (non-fluorescnt) and 3.2 µm (red fluorescent) particles in separate outlet channels was realized by 200 MHz TSAW. It is evident that most of the particles follow separate outlet ports during the separation, however, some particles are directed to the wrong port due to several unavoidable reasons. It is important to note that the two types of particles, already marginally different in size (with mean diameter 3.0 µm and 3.2 µm), have some variance in their sizes. Their defocused location inside the microchannel before entering the separation zone also contributes to some particles moving out through the wrong outlets. The imaging technique used here is similar to what described in the caption of Movie II.

Movie IV: The separation of 3.2 µm (red fluorescent) from 4.2 µm (non-fluorescent) particles in an almost stationary fluid is shown. The particles were first made to flow in a focused stream and then flow was suddenly stopped. The particles came to an approximate stand still position. The 155 MHz TSAW with 13 mW power were switched ON. The brighter fluorescent particles

were overcome by the streaming flow, whereas, the larger 4.2 µm particles were pushed in the rightward direction. The evident separation of the particles was confirmed by turning the microscope lamp ON and OFF.

Movie V: The TSAW having 155 MHz frequency were used to separate 3.2 µm (red fluorescent) from 4.2 µm (non-fluorescent) particles in a continuous flow. The separation of particles was realized at the net flow rates of 125 µL/h and 1,250 µL/h and the power inputs of 53 mW and 479 mW, respectively. The performance of the device was examined against time by continuously running the device for approximately 15 minutes. The separation was as good as was at the start of experiment. The particles sometimes appeared as distinguishable spots and sometimes as long streaklines because of variable exposure times used based on the need of the experiment.